

1 Recovery of stratigraphic data with associated uncertainties from drillhole databases using litho2strat
2 1.0

3 Vitaliy Ogarko^{1,2} and Mark Jessell^{1,2}

4 ¹Centre for Exploration Targeting (School of Earth Sciences), The University of Western Australia,
5 Crawley, 6009 WA, Australia

6 ²Mineral Exploration Cooperative Research Centre, The University of Western Australia, Crawley,
7 6009 WA, Australia

8 Correspondance: Vitaliy Ogarko (vitaliy.ogarko@uwa.edu.au)

9

10

11

Abstract

12

13 Australian commonwealth, state and territory geological surveys possess information on over 3 million
14 drillhole logs. In addition to mineral exploration drilling, extensive drillhole datasets exist from oil and
15 gas exploration and hydrogeological studies. Other countries no doubt have similar data holdings.
16 Together these legacy drillhole datasets have the potential to significantly improve our subsurface data
17 coverage but have limited use as constraints on regional 3D geological models as many if not most drill
18 logs lack stratigraphic information, containing only lithological descriptions.

19 This study develops open-source codes and methodologies for stratigraphy recovery (determining the
20 ordered sequence of stratigraphic units) from drillhole lithological data by introducing a search
21 algorithm that systematically explores all geologically plausible stratigraphic orderings for individual
22 drillholes, combined with a solution correlation algorithm that compares the topological relationships
23 of stratigraphic units across multiple drillholes to identify geologically consistent solutions and reduce
24 uncertainty. The algorithms combine constraints from lithological descriptions with stratigraphic
25 relationships automatically derived from regional maps. In addition, the method quantifies uncertainty
26 by generating multiple plausible stratigraphic interpretations, providing critical insights for resource
27 estimation, scenario analysis, and data acquisition strategies.

28 The application of our method to a dataset of 52 drillholes from South Australia demonstrated its
29 ability to make useful predictions of stratigraphic solutions and quantifying associated uncertainties.
30 These results not only validate our approach but also highlight opportunities to refine current
31 stratigraphic descriptions and provide a valuable new source for regional 3D geological modelling.

32

33

34 **1. Introduction**

35

36 Drillhole data serves as a fundamental constraint for subsurface geological exploration and 3D
37 geological modelling, offering direct insights into lithological and hence stratigraphic features
38 (Wellmann & Caumon, 2018). However, the inherent sparsity of such data, coupled with challenges
39 posed by legacy datasets maintained by industry and Geological Survey Organizations (GSOs), often
40 hinders comprehensive geological understanding and modelling (Jessell et al., 2010; Pakyuz-Charrier
41 et al., 2018). GSOs' databases typically contain lithological information as unstructured text
42 descriptions (e.g., 'sandy limestone with minor shale') but rarely include stratigraphic unit
43 assignments. This creates a critical gap in the data needed for accurate and meaningful geological
44 predictions (Hartmann & Moosdorf, 2012).

45 Geological modelling plays a crucial role in understanding subsurface structures and processes,
46 providing a foundation for various applications in earth sciences (Jessell et al., 2014). Such modelling
47 commonly relies on datasets such as borehole data, geophysical data, and mapping data. Among these,
48 borehole data provide the most accurate insights into subsurface geology and stratigraphy (Guo et al.,
49 2022). The models generated through geological modelling can serve dual purposes: they can be
50 directly employed for geological interpretations, such as identifying fault systems, and mineral
51 deposits (Alvarado-Neves et al., 2024; Vollgger et al., 2015), or they can be integrated as constraints in
52 methodologies that use a prior 3D model, such as geophysical inversions (Giraud et al., 2017; Martin
53 et al., 2024; Ogarko et al., 2021; Tarantola, 2005) and hydrogeological forward modelling (D'Afonseca
54 et al., 2020).

55 Modern drillhole measurement techniques primarily focus on chemical, mineralogical and lithological
56 characterization, whereas the fundamental categorical unit of regional 3D geological models is defined
57 by stratigraphy (Calcagno et al., 2008; Caumon et al., 2009; Mallet, 2002). This discrepancy
58 underscores the need for innovative approaches to recover and integrate stratigraphic information
59 from existing datasets.

60 Recent advancements in automation have made significant progress in processing drillhole data,
61 though most address different aspects of the problem than stratigraphic recovery. Data
62 standardization tools like dh2loop (Joshi et al., 2021) extract and harmonize lithological descriptions
63 from unstructured text using thesauri and fuzzy string matching, providing essential preprocessing for
64 downstream analysis. Pattern recognition methods (Schetselaar & Lemieux, 2012) can identify
65 lithostratigraphic markers and contacts within drill logs, helping to detect boundaries between units.
66 Machine learning approaches for 3D geological modeling (Guo et al., 2024) can interpolate between
67 drillholes to create subsurface models, but typically require pre-interpreted stratigraphic data as input.
68 While these methods provide valuable components of the workflow, none directly address the
69 fundamental challenge of transforming lithological descriptions into stratigraphic interpretations with
70 quantified uncertainties.

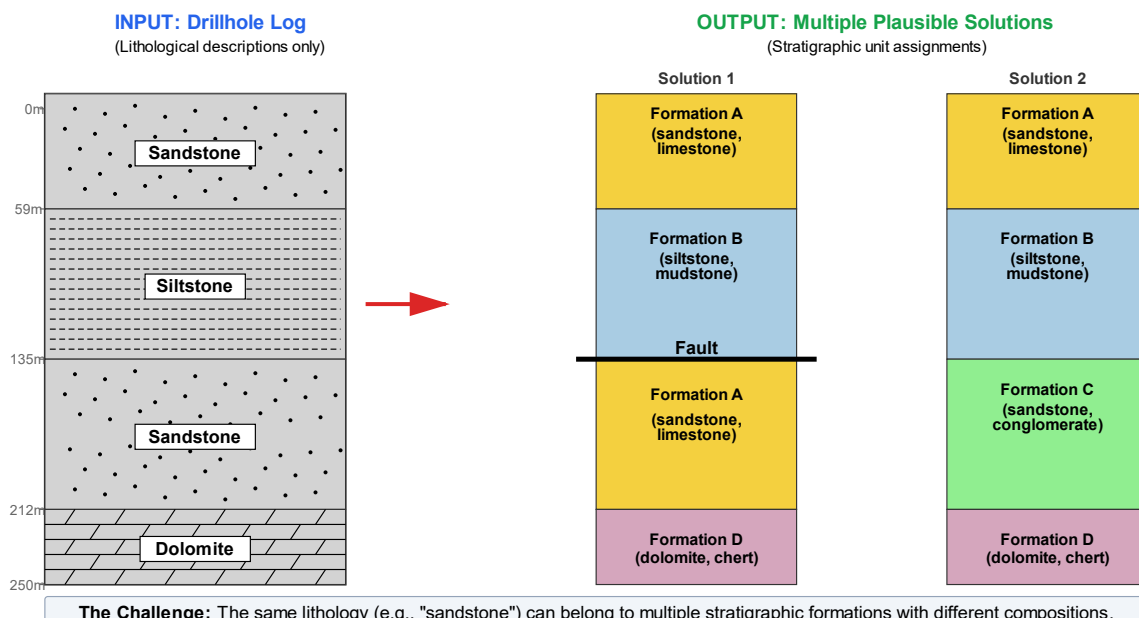
71 Existing automated interpretation methods primarily work with different data types than those
72 available in legacy drillhole databases. Geophysics-based methods (Wu & Nyland, 1987; Fullagar et al.,
73 2004; Silversides et al., 2015) leverage distinctive signatures in gamma, resistivity, or other wireline
74 logs to predict stratigraphic units, but require geophysical data that are absent from most legacy
75 drillholes. Geochemical and spectral approaches (Hill & Uvarova, 2018) use XRF scanning or
76 hyperspectral measurements to identify geological boundaries with high precision, but depend on
77 expensive data acquisition unavailable in historical datasets. Hybrid machine learning methods, such
78 as those applied in the Pilbara iron ore deposits (Wedge et al., 2019), combine lithology with assays

79 and geophysics but require extensive pre-interpreted drillhole datasets for training, limiting their
80 application in greenfield exploration areas. These approaches do not address the fundamental
81 challenge faced by geological surveys worldwide: millions of legacy drillholes contain only lithological
82 descriptions but lack both stratigraphic interpretations and the geophysical logs required by current
83 automated methods.

84 To address these challenges, we formulate the problem of stratigraphic recovery from drillhole
85 databases as follows. The input to our methodology consists of: (1) legacy drillhole databases
86 containing lithological descriptions (e.g., "sandstone", "siltstone", "dolomite") at various depth
87 intervals, typically without stratigraphic labels; (2) regional geological maps that define stratigraphic
88 unit boundaries and their spatial relationships; and (3) topological constraints that specify which
89 stratigraphic units can be in contact based on their known relative ages and depositional sequences.
90 The output comprises: (1) multiple plausible stratigraphic solutions, where each solution provides unit
91 assignments for all depth intervals in the drillholes; (2) their ranking by geological likelihood; and (3)
92 quantified uncertainties for these interpretations. The objective is threefold: first, to systematically
93 transform lithological descriptions into stratigraphic interpretations by testing all geologically plausible
94 orderings of stratigraphic units that are consistent with the observed lithologies; second, to quantify
95 the uncertainty inherent in these interpretations given that multiple stratigraphic units may share
96 similar lithological characteristics; and third, to establish correlations between multiple drillholes to
97 reduce uncertainty and improve the reliability of stratigraphic assignments across a region. This
98 transformation is essential because regional 3D geological models are fundamentally organized by
99 stratigraphy rather than lithology, yet the majority of legacy drillhole data lack stratigraphic labels.

100 Figure 1 illustrates this challenge with a simplified example: a drillhole log with four lithological
101 intervals (sandstone, siltstone, sandstone, dolomite) could correspond to multiple stratigraphic
102 interpretations. The two sandstone intervals might represent the same formation repeated by faulting,
103 or they could belong to different formations with similar but distinct lithological compositions. Without
104 additional constraints, both interpretations are geologically plausible, highlighting the inherent
105 ambiguity in stratigraphic assignment from lithological data alone.

The Challenge of Stratigraphic Interpretation from Lithological Data



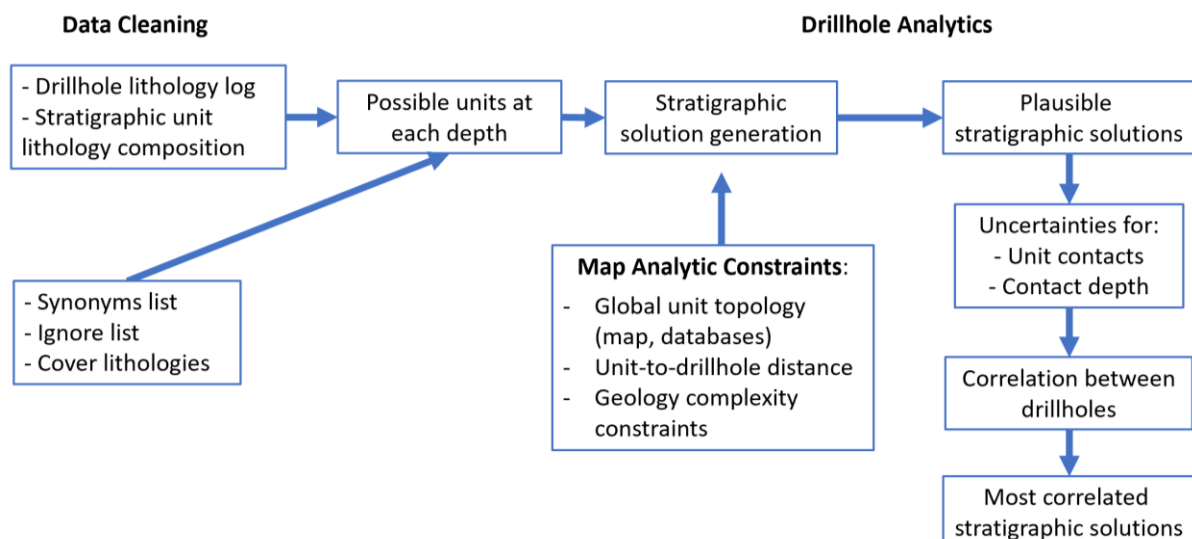
107 Figure 1: Schematic illustration of the stratigraphic interpretation problem. A drillhole log containing
108 only lithological descriptions (left) can yield multiple plausible stratigraphic solutions (right) because
109 the same lithology may occur in different stratigraphic formations with varying compositions.

110 This study develops open-source codes and methodologies for stratigraphy recovery from drillhole
111 lithological data through a two-stage approach. First, we introduce a branch-and-prune search
112 algorithm that systematically explores all geologically plausible stratigraphic orderings for individual
113 drillholes. Second, we apply a solution correlation algorithm that integrates information from multiple
114 drillholes by comparing topological relationships of stratigraphic units, thereby enhancing the
115 robustness and reliability of interpretations. The method quantifies uncertainty by generating multiple
116 plausible stratigraphic interpretations, providing critical insights for resource estimation, scenario
117 analysis, and data acquisition strategies. We apply our method to a dataset of 52 drillholes from South
118 Australia to demonstrate its practical application and validate its performance against existing
119 stratigraphic interpretations.

120 2. Methodology

121 2.1 Workflow

122



123

124 Figure 2: The different stages of the analysis.

125 The workflow shown in Fig. 2 consists of three key steps grouped into three main tasks: Data
126 Cleaning (using the dh2loop code), Map Analytic Constraints (using map2model and custom codes
127 developed for this project) and Drillhole Analytics (using the litho2strat code developed for this
128 project).

129

130 2.1.1 Data Cleaning

131 Prior to analysing the drillhole data we went through a number of automated data cleaning and
132 harmonisation steps.

133 a) Harmonisation of drillhole lithology descriptions using the dh2loop code described in (Joshi et
134 al., 2021) (code available here: <https://github.com/Loop3D/dh2loop>) This enables us to

135 produce a standardised lithological description for multiple drillholes in a region, regardless of
136 their provenance. This includes the use of a synonym list (“granite” vs “granitoid”), and ignore
137 list (e.g. “fault”) together with a list of cover lithology terms (e.g. “saprolite”) that enables us
138 to simplify the list of terms and exclude irrelevant information.

139

140 b) Harmonisation of lithological descriptions for formations described in the geological map of
141 the target area. This ensures that the same terminology is used for borehole lithological
142 descriptions and map lithologies.

143 Together steps a and b provide a list of possible units at each depth down a drill hole.

144

145 2.1.2 Map Analytic Constraints

146 a) Calculation of the distance between each polygon in a map and the target borehole. A custom
147 Python script was developed. This information can be used as a guide to the likelihood that a
148 drillhole would intersect a given unit.

149

150 b) We then used the map2model engine (M. Jessell et al., 2021) (code available here:
151 https://github.com/Loop3D/map2model_cpp) to extract the topological relationships
152 between the surface expression of stratigraphic different units. This would later be used to
153 assess the likelihood that two units would be in contact in the drillhole.

154 The map2model engine extracts topological relationships between stratigraphic units,
155 including both normal depositional contacts and fault contacts, as both types of juxtaposition
156 may be encountered in drillhole data.

157

158 Unit connectivity information can also be obtained from the Australian Stratigraphic Units
159 Database (ASUD) as well as from various published reports containing stratigraphic data. The
160 ASUD serves as a comprehensive repository of geological information, providing valuable
161 insights into the relationships between different stratigraphic units across Australia.
162 Additionally, numerous geological surveys and research studies offer stratigraphic data that
163 can further enrich our understanding of unit connectivity. Leveraging this information,
164 enhances stratigraphic models, improves the accuracy of correlations between drillholes, and
165 facilitates a deeper understanding of the geological framework in specific regions.

166

167 These two steps allow us to capture information on the spatial and topological relationships
168 between the mapped units.

169

170 2.1.3 Drillhole Analytics

171 In this stage, we employ the litho2strat code to generate plausible stratigraphic solutions that fit
172 the observed lithological data while satisfying all geological constraints (code available here:
173 <https://github.com/Loop3D/litho2strat>; Ogarko et al., 2025). The algorithm uses a recursive
174 branch and prune approach to efficiently explore the solution space, eliminating geologically
175 implausible pathways early in the search process (see Section 2.2 for detailed algorithm
176 description). This strategy not only ensures thorough exploration of viable stratigraphic orderings
177 but also optimizes computational efficiency by avoiding unnecessary enumeration of invalid
178 solutions.

179 From the complete ensemble of plausible solutions obtained for each drillhole, we calculate
180 uncertainties that quantify the confidence in different stratigraphic interpretations. Solutions are
181 scored based on the probability of unit contacts within the local solution ensemble, providing a
182 ranking of stratigraphic hypotheses from most to least likely.

183 To further reduce uncertainty and improve solution reliability, we implement a correlation
184 algorithm that leverages information from multiple neighboring drillholes simultaneously (see
185 Section 2.5 for correlation algorithm details). By comparing the topological relationships of
186 stratigraphic units across drillholes, the correlation process identifies solutions that are
187 geologically consistent across the broader area. Correlated solution scores integrate both local
188 evidence from individual drillholes and regional consistency with neighboring holes, with
189 solutions receiving the highest correlated scores selected as the most plausible stratigraphic
190 interpretations.

192 2.2 Stratigraphic solution generation

193

194 The litho2strat algorithm operates through a hierarchical search strategy that systematically explores
195 the space of possible stratigraphic orderings (solutions) while pruning geologically implausible
196 solutions. The algorithm can be formally described as follows:

197 **Input:**

- 198 • $L = \{l_1, l_2, \dots, l_n\}$: sequence of lithologies observed at depths $d_1 < d_2 < \dots < d_n$
- 199 • $U = \{u_1, u_2, \dots, u_m\}$: set of m candidate stratigraphic units, each defined by its constituent
200 lithologies
- 201 • C : set of geological constraints (distance, connectivity, complexity)
- 202 • Γ : global unit connectivity graph derived from geological maps and stratigraphic databases

203 **Output:**

- 204 • $S = \{s_1, s_2, \dots, s_k\}$: set of k plausible stratigraphic solutions
- 205 • $P(s_i)$: probability distribution over solutions
- 206 • G_h : local connectivity graph for drillhole h , derived from all solutions for this drillhole

207 **Algorithm Steps:**

208 **1. Unit Matching Phase:** For each lithology l_i at depth d_i , identify the subset of compatible units:

$$209 M(l_i) = \{u_j \in U \mid \text{lithology}(u_j) \text{ matches } l_i \text{ AND satisfies constraints } C\}$$

210 **2. Recursive Branch and Prune Exploration:** The algorithm recursively builds the solution space from
211 shallow to deep depth intervals. Starting from the surface, partial solutions are extended one depth
212 level at a time by considering candidate units that match the observed lithology. The algorithm
213 generates a new branch for candidate unit u_j only when all of the following conditions are satisfied:

- 214 • The unit u_j matches the observed lithology at the current depth
- 215 • The extended solution satisfies all constraints in C (distance, occurrence, contact complexity)

216 • For the last unit u_k in the partial solution, the edge (u_k, u_j) exists in the global connectivity
 217 graph Γ

218 Partial solutions that violate any condition are immediately abandoned (pruned), preventing
 219 exploration of their extensions. When a partial solution reaches the deepest depth interval, it is
 220 validated and added to the solution set S . This recursive approach with constraint-based pruning
 221 eliminates large portions of the solution space without explicit enumeration.

222 The algorithm systematically explores all geologically valid solutions through exhaustive search with
 223 constraint-based pruning. While the top-to-bottom traversal order does not affect the completeness
 224 of the final solution set S (the same valid stratigraphic interpretations would be found regardless of
 225 traversal direction), it does improve computational efficiency by enabling earlier application of
 226 surface geology constraints and more effective pruning of invalid solution branches.

227 **3. Local Connectivity Graph Construction:** From the complete set of solutions S obtained for drillhole
 228 h , construct a local connectivity graph G_h where edge weights represent the frequency of unit
 229 contacts across all solutions:

230 $w_h(u_j, u_{j+1}) = |\{s \in S : (u_j, u_{j+1}) \text{ adjacent in } s\}| / |S|$

231 This directed local graph captures the probability of unit contacts based on the ensemble of
 232 geologically plausible solutions for drillhole h , where edges represent stratigraphic ordering. Each
 233 edge weight represents the fraction of solutions in which the corresponding unit contact appears.
 234 Note that G_h is a subgraph of the global connectivity graph Γ , as all solutions for drillhole h must
 235 satisfy the global connectivity constraints.

236 **4. Solution Scoring:** For each solution $s_i \in S$, calculate a normalized score based on the local
 237 connectivity graph G_h :

238 $score(s_i) = \sum_j w_h(u_j, u_{j+1}) / N_i$

239 where N_i is the number of unit contacts in solution s_i (i.e., $N_i = |s_i| - 1$), and the sum is over all
 240 consecutive unit pairs. The normalization by N_i ensures that solutions with different numbers of
 241 stratigraphic contacts are directly comparable, preventing bias toward longer or more complex
 242 solutions. The score thus represents the average edge probability across all contacts in the solution.

243 **5. Probability Calculation:** Normalize scores to obtain probability distribution:

244 $P(s_i) = score(s_i) / \sum_k score(s_k)$

245 The efficiency of this approach derives from constraint-based pruning during the recursive
 246 exploration. By evaluating both solution constraints C and global connectivity Γ before extending
 247 each partial solution, the algorithm eliminates inconsistent paths immediately without exploring
 248 their complete extensions. The distinction between the global connectivity graph Γ (used for
 249 constraint validation during exploration) and the local connectivity graph G_h (derived from solutions
 250 and used for scoring) is crucial: Γ represents *a priori* geological knowledge from maps and databases,
 251 while G_h captures the *a posteriori* probability distribution of unit contacts specific to drillhole h given
 252 all constraints.

253

254 [2.3 Solution constraints](#)

255

256

257 For the Branch and Prune algorithm described in Section 2.2, providing efficient constraints
258 (collectively denoted as C) is crucial for generating geologically plausible stratigraphies and reducing
259 the search space. Without these constraints, the algorithm would need to exhaustively enumerate all
260 possible unit assignments, which is computationally prohibitive. We utilize two types of solution
261 constraints: the first can be derived from geological maps (as discussed in the 'Map Analytic
262 Constraints' section), while the second is selected by the user based on the expected structural
263 complexity of the area (e.g., the presence of faults, folds, or other features that might cause
264 stratigraphic repetition or disruption).

265 **The specific constraints in C include:**

266 **1. Distance Constraint:** This constraint limits the number of geological units considered based on
267 their proximity to the drillhole. In this context this is defined as the distance between the drillhole
268 collar and the nearest point on the polygon's boundary in 2D. For drillhole h and candidate unit $u_j \in$
269 U :

270 $d(u_j, h) \leq dmax$,

271 where $d(u_j, h)$ is the distance from the nearest outcrop of unit u_j to drillhole h , and $dmax$ is the
272 maximum search radius. This ensures relevance to the drillhole's location.

273 **2. Global Unit Connectivity Constraint:** This constraint, enforced through the global connectivity
274 graph Γ , restricts potential contacts between units. For any two consecutive units u_j and u_{j+1} in a
275 solution:

276 $(u_j, u_{j+1}) \in E(\Gamma)$,

277 where $E(\Gamma)$ is the edge set of the global connectivity graph. This ensures that only units known to be
278 stratigraphically adjacent (from map data, databases, or published reports) can be placed in contact,
279 enhancing the geological plausibility of solutions.

280 The edges in the global connectivity graph Γ can be configured as either single-directional or
281 bidirectional depending on the structural complexity of the study area. In structurally simple areas
282 with normal stratigraphic succession, single-directional edges (e.g., A→B) enforce the expected
283 younging direction (older to younger upward). However, for areas with known structural complexities
284 such as overturned sequences from folding or thrust faulting, bidirectional edges can be used to
285 allow stratigraphic contacts in both normal and reversed orientations. For example, if units A and B
286 can occur in both normal succession (A overlies B) and overturned succession (B overlies A) due to
287 folding, the graph Γ would include a bidirectional edge between them, allowing transitions in both
288 directions (A→B and B→A). This configuration allows the algorithm to exhaustively explore all
289 structurally valid solutions including those with reversed polarity sequences. The choice of single-
290 directional versus bidirectional edges in Γ is thus a key input that controls whether the algorithm
291 considers only normal superposition or also accommodates structural inversions.

292 **3. Top Unit Constraint:** Information regarding the top unit $utop$ can be extracted from geological
293 maps at the surface location of the drillhole, providing a foundational boundary condition:

294 $s[0] = utop$,

295 where $s[0]$ denotes the shallowest unit in solution s . Note that while the global unit connectivity
 296 constraint allows sequences to begin from any node in the connectivity graph, this constraint
 297 explicitly specifies the starting node.

298 **4. Occurrence Constraint:** This constraint sets a maximum limit on how many times a unit can appear
 299 in a solution, accounting for geological complexity such as faulting or folding. For unit u_j in solution s_i :
 300 $count(u_j, s_i) \leq kmax$,
 301 where $count(u_j, s_i)$ is the number of times unit u_j appears in s_i . Typically $kmax = 1$ for unfaulted
 302 sequences, or $kmax = 2-3$ for faulted terrains where stratigraphic repetition may occur.

303 **5. Contact Complexity Constraint:** For a continuous sequence of identical lithology observations $[l_i, l_{i+1}, \dots, l_{i+m}]$ where all lithologies are the same, this constraint limits the number of distinct
 304 stratigraphic units that can be assigned:
 305 $|\{u_j : assigned to interval [i, i+m]\}| \leq cmax$,
 306 where $cmax$ is the maximum number of unit contacts allowed within the continuous lithology
 307 sequence. This prevents over-interpretation where a thick monotonous lithology (e.g., a 100m
 308 sandstone sequence) is artificially divided into an excessive number of stratigraphic units.

309 **6. Stratigraphic Jump Constraint:** To account for incomplete exposure of geological contacts at the
 310 surface, we allow the algorithm to "jump" over intermediate units in the global connectivity graph Γ .
 311 For a path in Γ such as $A \rightarrow B \rightarrow C$, setting the maximum number of stratigraphic jumps parameter to
 312 $jmax$ allows direct contacts between non-adjacent units up to $jmax$ steps apart in the graph. For
 313 example, with $jmax=1$, the algorithm can consider both $A \rightarrow B$ and $A \rightarrow C$ as valid contacts, even if $A \rightarrow C$
 314 is not explicitly observed in the map data. This addresses the limitation that geological maps provide
 315 only a 2D surface expression of 3D geological relationships and may not capture all possible
 316 stratigraphic contacts that exist at depth. The constraint is defined as:
 317

318 $d\Gamma(ui, uj) \leq jmax + 1$
 319 where $d\Gamma(ui, uj)$ is the shortest path distance between units ui and uj in the connectivity graph Γ , and
 320 $jmax$ is the maximum number of allowed jumps (typically $jmax=0$ for strict adherence to observed
 321 contacts, or $jmax=1-2$ for more permissive exploration).

322 These constraints in C work together to enhance the efficiency and effectiveness of the Branch and
 323 Prune algorithm, ensuring that the resulting stratigraphies are both geologically plausible and
 324 computationally tractable. As demonstrated in Section 3, constraint-based pruning reduces the
 325 search space by >99% in practical applications, enabling computation of all valid solutions in seconds.

326

327 [2.4 Computational complexity](#)
 328

329 The computational complexity of the branch and prune algorithm depends on several key factors:
 330 the number of drillholes H , the length of the lithology sequence $|L|$ (i.e., the number of depth
 331 intervals), the number of candidate stratigraphic units $|U|$, and critically, the average number of
 332 solutions N maintained during the recursive exploration. The algorithm processes each drillhole
 333 independently, and for each drillhole, it iterates through all lithologies in L , evaluating potential unit
 334 assignments for each active solution.

335 The theoretical time complexity can be expressed as:
 336 $O(H \times |L| \times N \times |U|)$
 337 where N denotes the average number of solutions maintained during recursive exploration. This is
 338 the most variable factor and depends strongly on the geological complexity and the constraints
 339 applied.
 340 In the unconstrained case, where no geological constraints are imposed, the number of solutions can
 341 grow exponentially with the number of lithology changes k in the drillhole log, potentially reaching N
 342 $\propto |U|^k$. This leads to a worst-case complexity of $O(H \times |L| \times |U|^{k+1})$, which quickly becomes
 343 computationally prohibitive for complex stratigraphic sequences.
 344 However, the application of geological constraints C - particularly the global unit connectivity
 345 constraint enforced through the topology graph Γ - dramatically reduces the solution space. These
 346 constraints prune geologically implausible branches early in the recursive exploration, preventing
 347 exponential growth of N . In practice, with appropriately chosen constraints, N grows moderately with
 348 the number of lithology changes (approximately linearly rather than exponentially), resulting in
 349 manageable computational requirements even for complex stratigraphic sequences.
 350 The effectiveness of constraint-based pruning in controlling computational cost is demonstrated
 351 empirically in Section 3, where we compare the growth of average solution numbers as a function of
 352 lithology changes for cases with and without topology constraints.

353
 354 [2.5 Solution correlation](#)
 355 We utilize solution correlation analysis to identify compatible stratigraphic orderings between
 356 multiple drillholes, serving as a constraint on the plausibility of individual solutions. This correlation
 357 leverages the topological relationships of units represented through local connectivity graphs from
 358 each drillhole.
 359 A key challenge in correlating stratigraphy logs is that units at the same depth may not align across
 360 different drillholes due to variations in unit dip and thickness, tectonic deformation, and stratigraphic
 361 gaps (such as unconformities or erosional surfaces). To address this, we focus on correlation based
 362 on topological relationships rather than depth-matching. The local connectivity graph G_h for each
 363 drillhole h is constructed from the complete set of solutions S_h obtained via the Branch and Prune
 364 algorithm (Section 2.2), where nodes represent geological units, edges represent stratigraphic
 365 ordering between units, and edge weights $w_h(u_j, u_{j+1})$ represent the probability of unit contacts
 366 within that drillhole's solution ensemble.
 367 To facilitate correlation analysis, we generalize the scoring function from Section 2.2 to evaluate any
 368 solution s_i against any local connectivity graph. Define the generalized scoring function as:
 369 $score(s_i, G_h) = \sum_j w_h(u_j, u_{j+1}) / N_i$,
 370 where the sum is over all consecutive unit pairs (u_j, u_{j+1}) in solution s_i , G_h represents any local
 371 connectivity graph derived from drillhole solutions, $w_h(u_j, u_{j+1})$ denotes the edge weight from graph
 372 G_h for that unit pair, and N_i is the number of unit contacts in solution s_i . Note that G_h refers to local
 373 connectivity graphs from drillhole solutions, not the global connectivity graph Γ from map data
 374 (Section 2.2). If an edge (u_j, u_{j+1}) from solution s_i does not exist in G_h , its weight is taken as zero. This

375 generalized function allows us to assess how consistent a solution from one drillhole is with the
376 geological relationships observed in other drillholes.

377 **Correlation Algorithm:**

378 Consider a set of H drillholes $\{h_1, h_2, \dots, h_H\}$ with their respective local connectivity graphs $\{G_1, G_2, \dots, G_H\}$. For each solution s_i from any drillhole, we compute a correlated score that represents the
379 average consistency across all drillholes:

381
$$scorecorr(s_i) = (1/H) \sum_{k=1}^H \alpha_k score(s_i, G_k),$$

382 where α_k are weighting factors that can be based on geological distance (distance between collar and
383 closest node of map polygon), drillhole quality, or other criteria. This equation computes an average
384 score across all drillholes. The division by H ensures the correlated score remains on a comparable
385 scale regardless of the number of drillholes. In this work, we use $\alpha_k = 1$ for all drillholes, giving equal
386 weight to each drillhole. This summation approach is robust to outliers; if one drillhole yields a zero
387 score, it does not eliminate the entire correlation. Alternative weighting schemes such as $\alpha_k = 1/d(h_i, h_k)$
388 could be employed to reduce the influence of more distant drillholes.

389 The correlated scores are then normalized to obtain a revised probability distribution:

390
$$Pcorr(s_i) = scorecorr(s_i) / \sum_m scorecorr(s_m),$$

391 The correlated probability $Pcorr(s_i)$ provides a revised ranking of solutions that accounts for both
392 local evidence and regional consistency. Solutions with unit contacts that appear frequently across
393 multiple drillholes receive higher correlated scores, while solutions unique to a single drillhole
394 receive lower scores. This correlation effectively reduces uncertainty by leveraging spatial geological
395 consistency.

396 **Summation vs. Multiplication:** While the equation for $scorecorr$ uses weighted summation, an
397 alternative multiplicative approach could also be formulated. However, multiplicative forms are more
398 sensitive to outliers: if any single drillhole yields a zero score, the entire correlated score becomes
399 zero. Therefore, the summation approach is generally preferred for its robustness.

400 **Computational Efficiency:** The algorithm achieves $O(H^2|S|)$ complexity when correlating solutions
401 across all n drillholes. This efficiency is achieved by comparing solutions against pre-computed
402 connectivity graphs G_h rather than individual solutions. The alternative of solution-to-solution
403 comparison would scale as $O(H^2|S|^2)$ and be computationally prohibitive.

404 By integrating and correlating drillhole data through this topological approach, we ensure that the
405 stratigraphic framework accurately reflects the natural spatial variations and interconnections
406 present in the subsurface. The correlation process quantitatively reduces uncertainty by identifying
407 and favoring solutions that are geologically consistent across the broader area. This uncertainty
408 reduction is achieved by concentrating probability mass on solutions supported by multiple drillholes
409 while downweighting locally anomalous interpretations. The resulting correlated probabilities
410 $Pcorr(s_i)$ provide more reliable stratigraphic interpretations than single-drillhole probabilities $P(s_i)$,
411 enabling more informed decisions in geological exploration and 3D geological modeling.

412

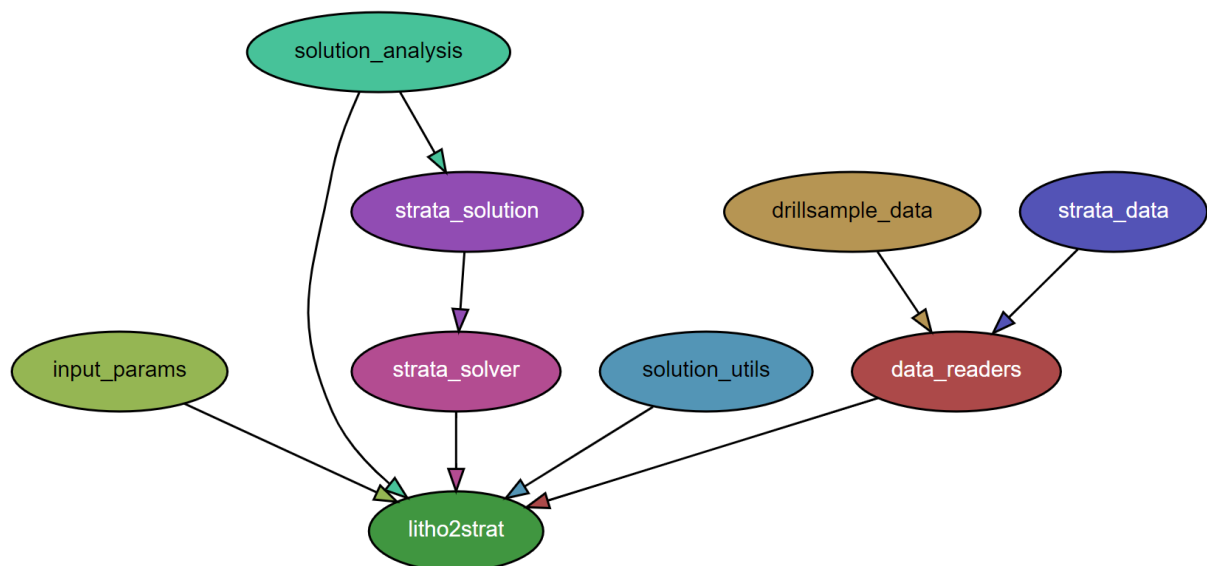
413 [2.6 Code design](#)

414

415 A Python package called *litho2strat* has been developed for stratigraphy recovery. It can be easily
416 installed using the command “*pip install*”, and it has minimal external library dependencies: *numpy*,
417 *matplotlib*, and *NetworkX*. The *NetworkX* library is utilized to create a directed graph data structure
418 that represents the topological relationships of relative unit ages (Hagberg et al., 2008). It also
419 supports exporting graphs to *GML* format (Himsolt, 1997) for advanced graph visualization with tools
420 like *yEd* (<https://www.yworks.com/products/yed>).

421 Interaction with the code is facilitated through a *Parfile*, a text file that contains all necessary
422 parameters and paths to the input data files. The parameters in the *Parfile* are organized into several
423 categories based on their functionality, including input file paths, solver settings, and data
424 preprocessing options. An example of such a *Parfile* is provided in Appendix A.

425 The code architecture efficiently organizes distinct modules, including data reader, the user interface
426 (represented by the *Parfile*), the algorithms (such as the solver), and the visualization components
427 (e.g., output figures and graphs), as shown in Fig. 3. This design enhances code readability, making it
428 easier for developers to understand and navigate the codebase. Additionally, it facilitates further
429 extensions by allowing new features to be integrated seamlessly. This structure also supports
430 effective testing, enabling modifications to be verified systematically and reducing the risk of
431 introducing errors..



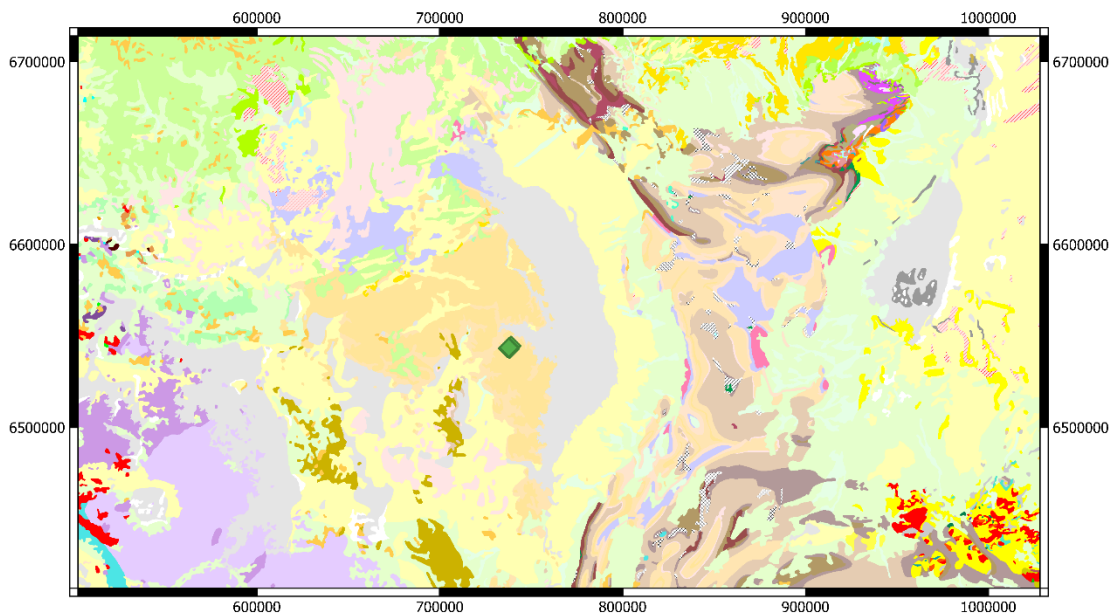
432

433 Figure 3: The module dependencies of the *litho2strat* code. The graph is generated by the *pydeps*
434 utility, while excluding external dependencies.

435 3. Example Use

436

437 For this example, we used a set of 52 drillholes from South Australia originally drilled by Teck
438 Cominco Pty. Ltd. (Fig. 4). This area was chosen as there were a number of holes equally spaced with
439 a relatively homogenous spatial distribution and the holes provided both lithological logs and
440 existing interpretations of the down-hole stratigraphy.



441

442

443 Figure 4: Location of South Australia test area (drillholes shown as green diamonds), together with an
 444 example stratigraphic log, map from 1:2M Surface Geology Map of South Australia (The Department
 445 for Energy and Mining, the Government of South Australia, Geoscientific. Data, Sourced on 22 July
 446 2018, [http://energymining.sa.gov.au/minerals/geoscience/geological_survey/data_GDA94/Zone 53](http://energymining.sa.gov.au/minerals/geoscience/geological_survey/data_GDA94/Zone_53)).

447 **Data Cleaning**

448

449 Examples of terms in the ignore list for this case study include the following, where each term is
 450 excluded from drillhole lithology log processing:

- 451 1. Breccia (Undiff. Origin)
- 452 2. Ironstone (Metasomatic)
- 453 3. No Information
- 454 4. Solution-Collapse Breccia
- 455 5. Vein (Undifferentiated)

456

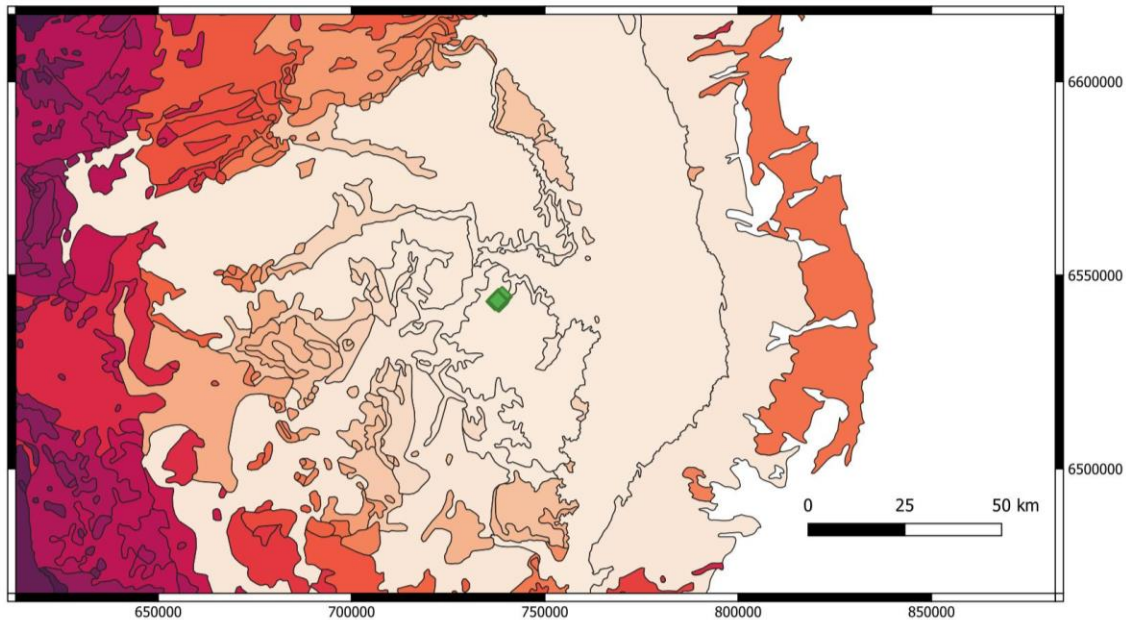
457 Examples of the thesaurus of synonyms for this case study area include the following groups, where
 458 each group contains lithology names that are treated as equivalent:

- 459 1. dolomite, dolomite rock, carbonate rock, limestone
- 460 2. conglomerate, diamictite
- 461 3. grit, sandstone, quartzite, siltstone
- 462 4. gabbro, gabbronorite

463

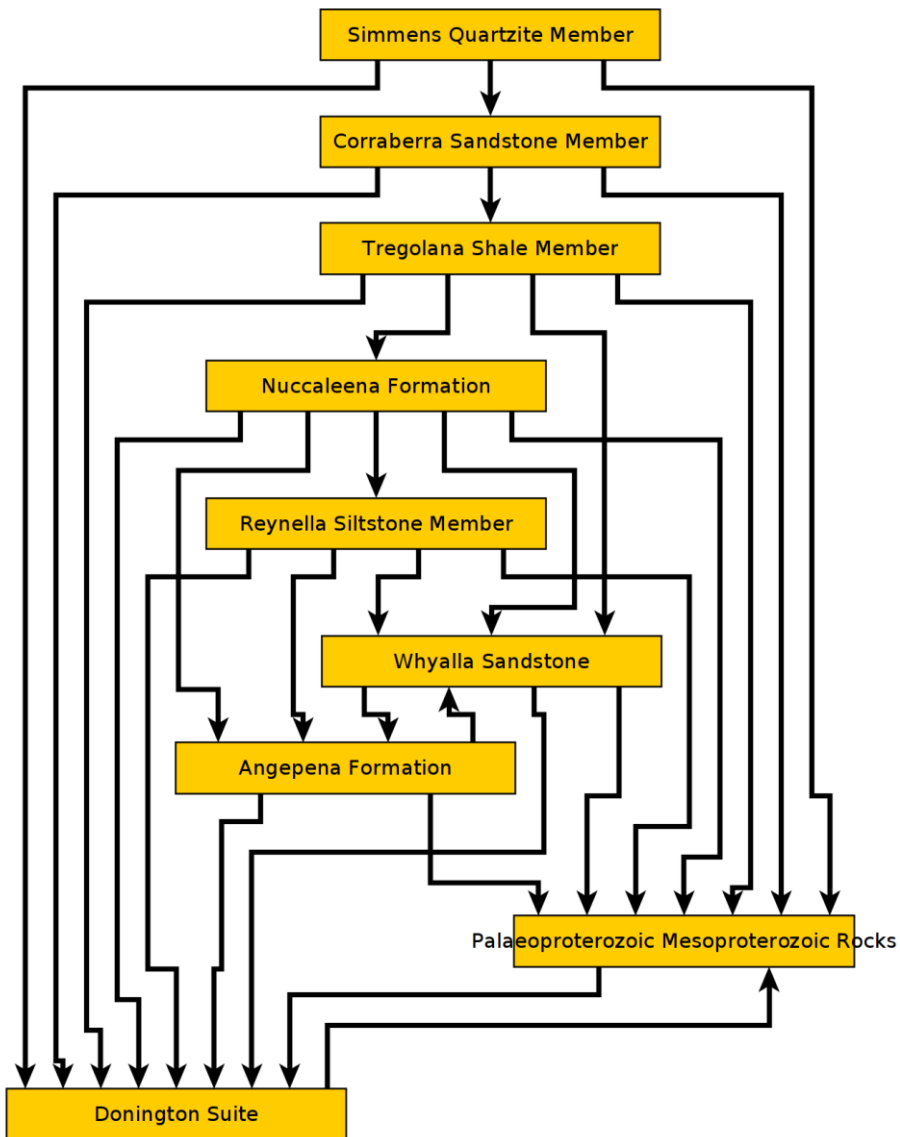
464 **Map Analytics**

465 Figure 5 shows stratigraphic units coloured as a function of the distance to one of the drillholes. A
466 large search area was used for this example as the stratigraphy is fairly flat lying so there is no
467 guarantee that a unit will reach the surface in the local neighbourhood.



468
469 Figure 5. Distance of stratigraphic units from drillholes (darker colours signifies larger distance).
470 Green diamonds show the location of the drillholes (Same source map as Fig. 4, GDA94/Zone 53).
471 In the initial analysis we constructed the global connectivity graph Γ (Section 2.2), representing
472 topological relationships between stratigraphic units. The initial graph was constructed automatically
473 from the geology map (extending out 100 km from the test area) using the map2model software, then
474 manually extended with additional topological relationships from the ASUD database and published
475 reports. The graph was processed using the NetworkX Python library, exported to GML format, and
476 visualized using yEd software (Fig. 6). The global connectivity graph consists primarily of single-
477 direction edges, with two bidirectional edges (Whyalla Sandstone–Angepena Formation and
478 Paleoproterozoic–Mesoproterozoic Rocks–Donington Suite) to account for spatial variability in their
479 stratigraphic relationships.

480



481

482

Figure 6: Topological relationships between units in and around the test area.

483

484

485 **Drillhole Analytics**

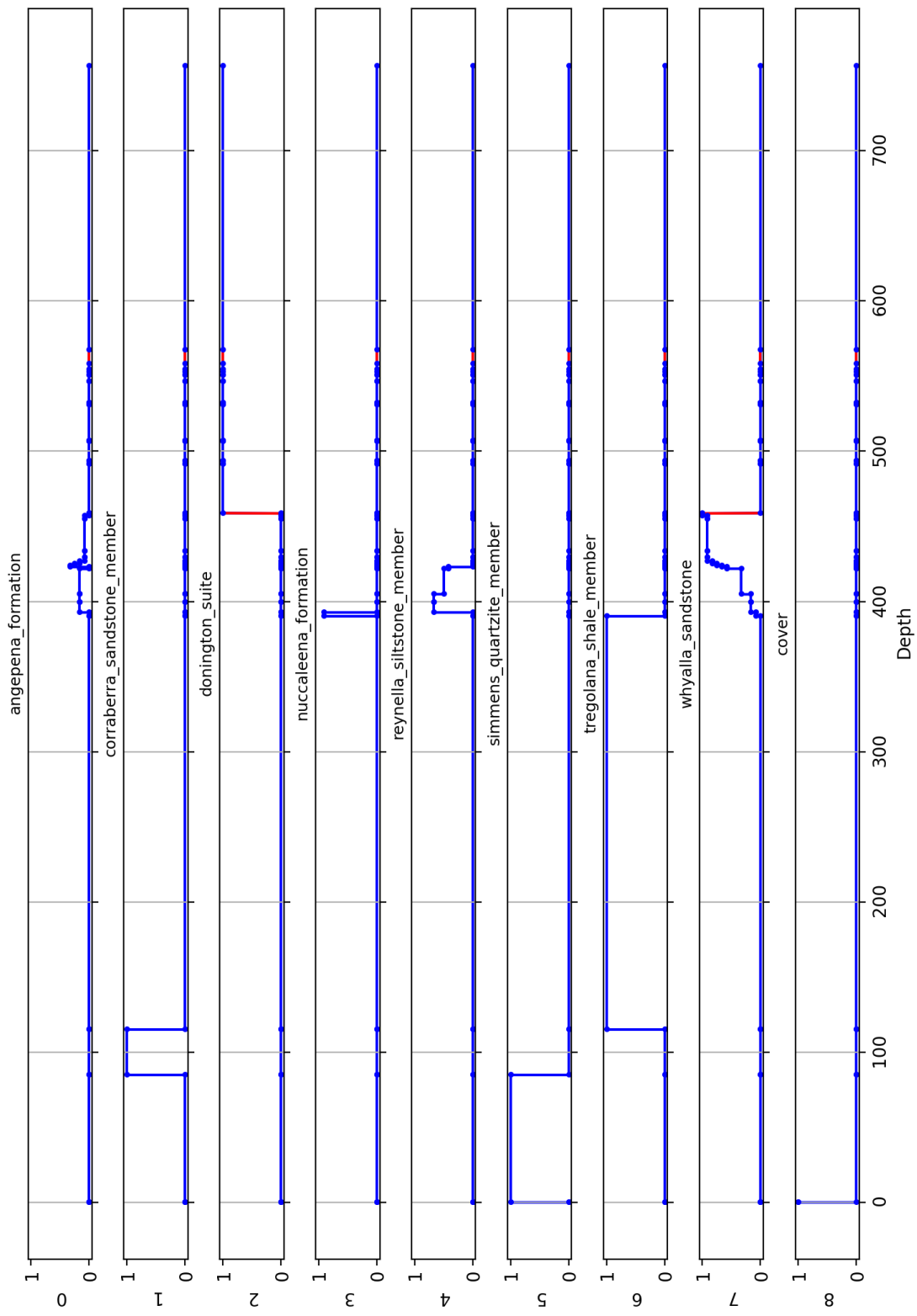
486 The drillhole analysis calculated every possible stratigraphic ordering that was consistent with the
 487 observed lithological ordering down the drillhole and solution constraints (described in Sec. 2.3). By
 488 collating the results for all possible solution paths, we can produce estimates of the marginal
 489 probability that any depth interval will be a particular stratigraphic unit (Fig. 7). For depth interval i
 490 and stratigraphic unit u , the probability $P_{-i}(u)$ is computed as:

491
$$P_{-i}(u) = |\{s \in S : s[i] = u\}| / |S|,$$

492 where S is the set of all valid solutions and $s[i]$ denotes the unit assigned to interval i in solution s .

493

494
495 Probability of occurrence for every unit. CollarID = 265003
496

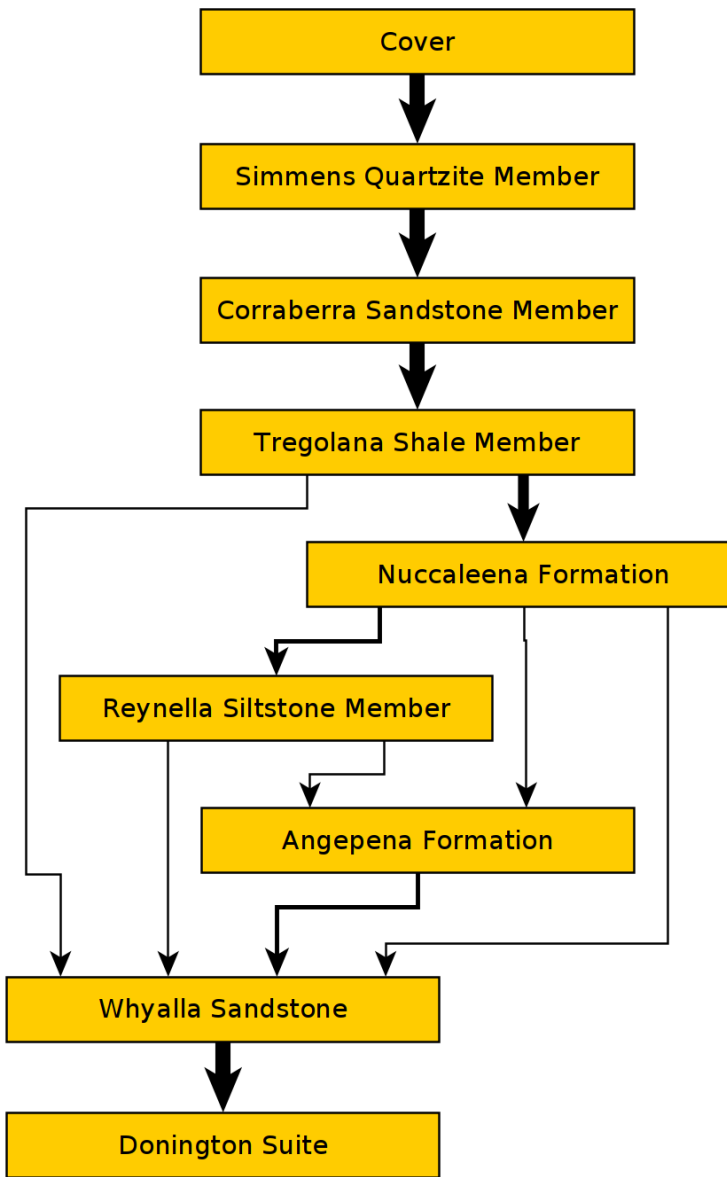


494

495 Figure 7: Estimated probability of each stratigraphic unit occurring at a given depth for a single
496 drillhole.

497 In Fig. 8, we present the final (local) unit connectivity derived from the stratigraphic solutions
498 generated. The width of the graph edges indicates the probability of unit contacts, with thicker edges

499 signifying higher probabilities. This visual representation allows for a clear comparison of
500 connectivity before (Fig. 6) and after the stratigraphic analysis.



501
502 Figure 8: Calculated local topology using all solutions. Graph edges (relationships) between two
503 stratigraphic units are displayed as a probability of a that contact-relationship occurring.

504 The final solution score for a single ordering is calculated by summing of the probabilities of the
505 contact edge weights. This allows us to sort the orderings by probability, ignoring stratigraphic
506 thickness for now (Fig. 9).

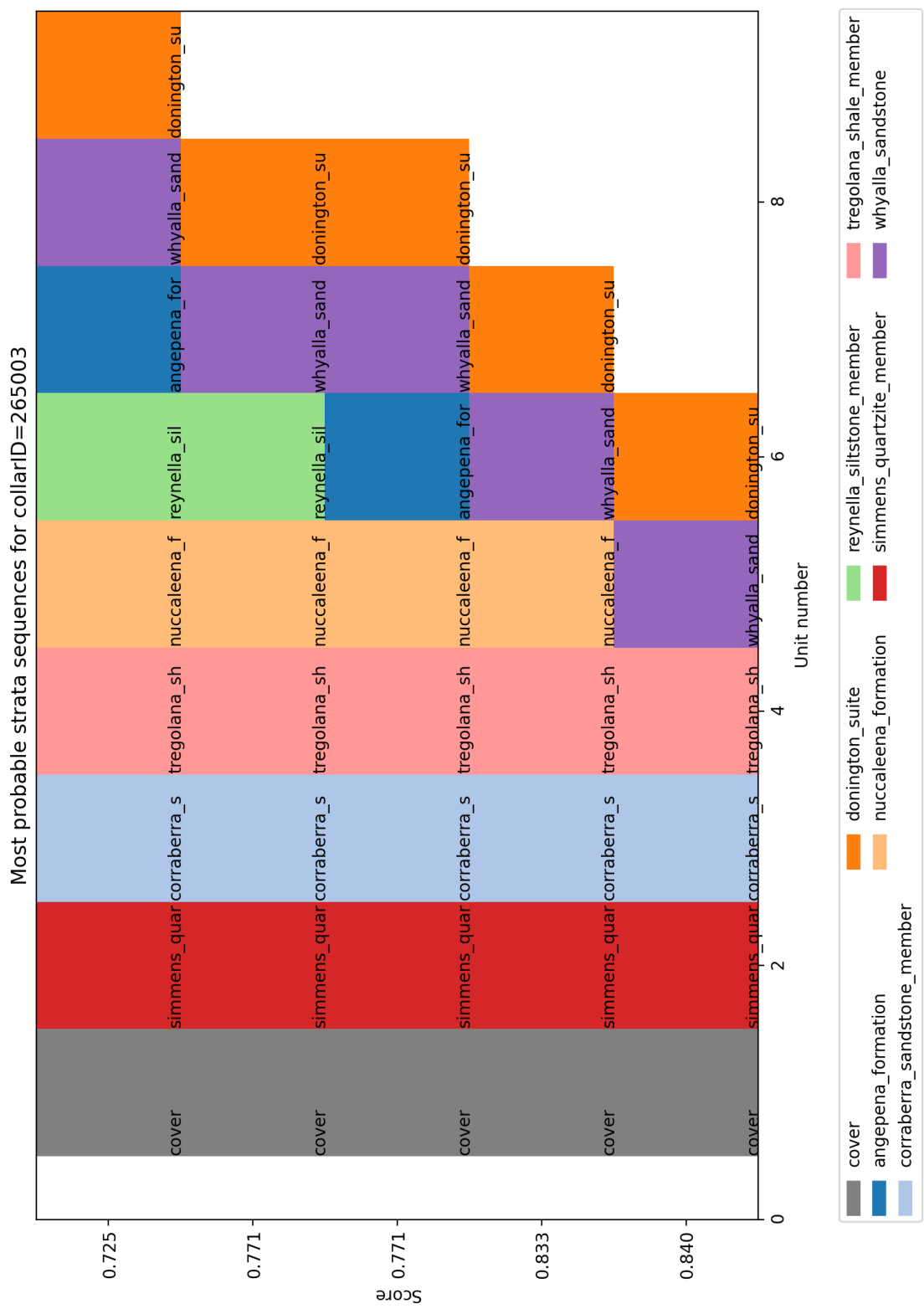
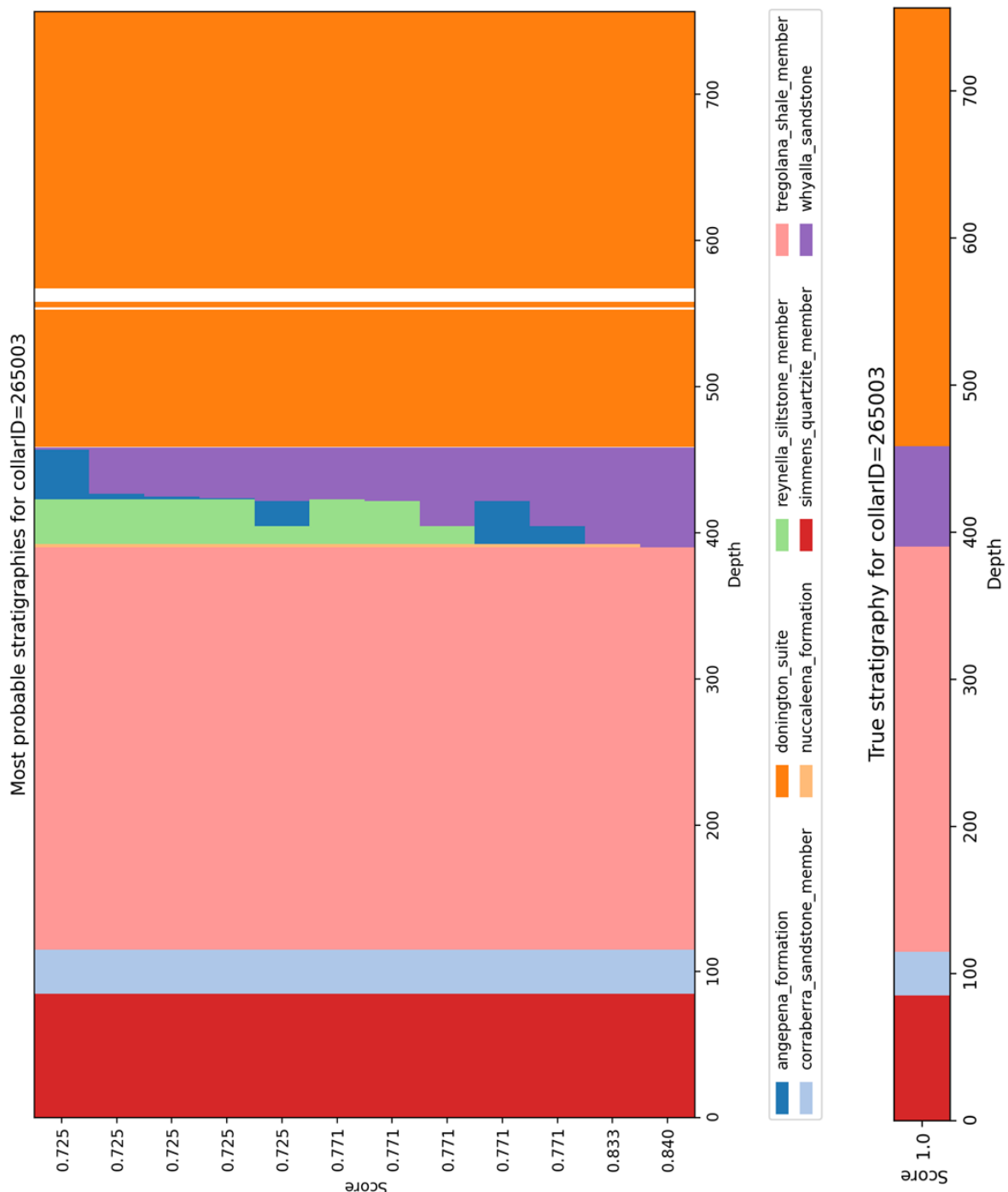


Figure 9: The 5 most probable stratigraphic orderings, with their solution probability on the x axis and order of depth on the y axis.

511 Finally, we can then include the depths to contacts between units in the drillhole based on the
512 previous analyses (Fig. 10).

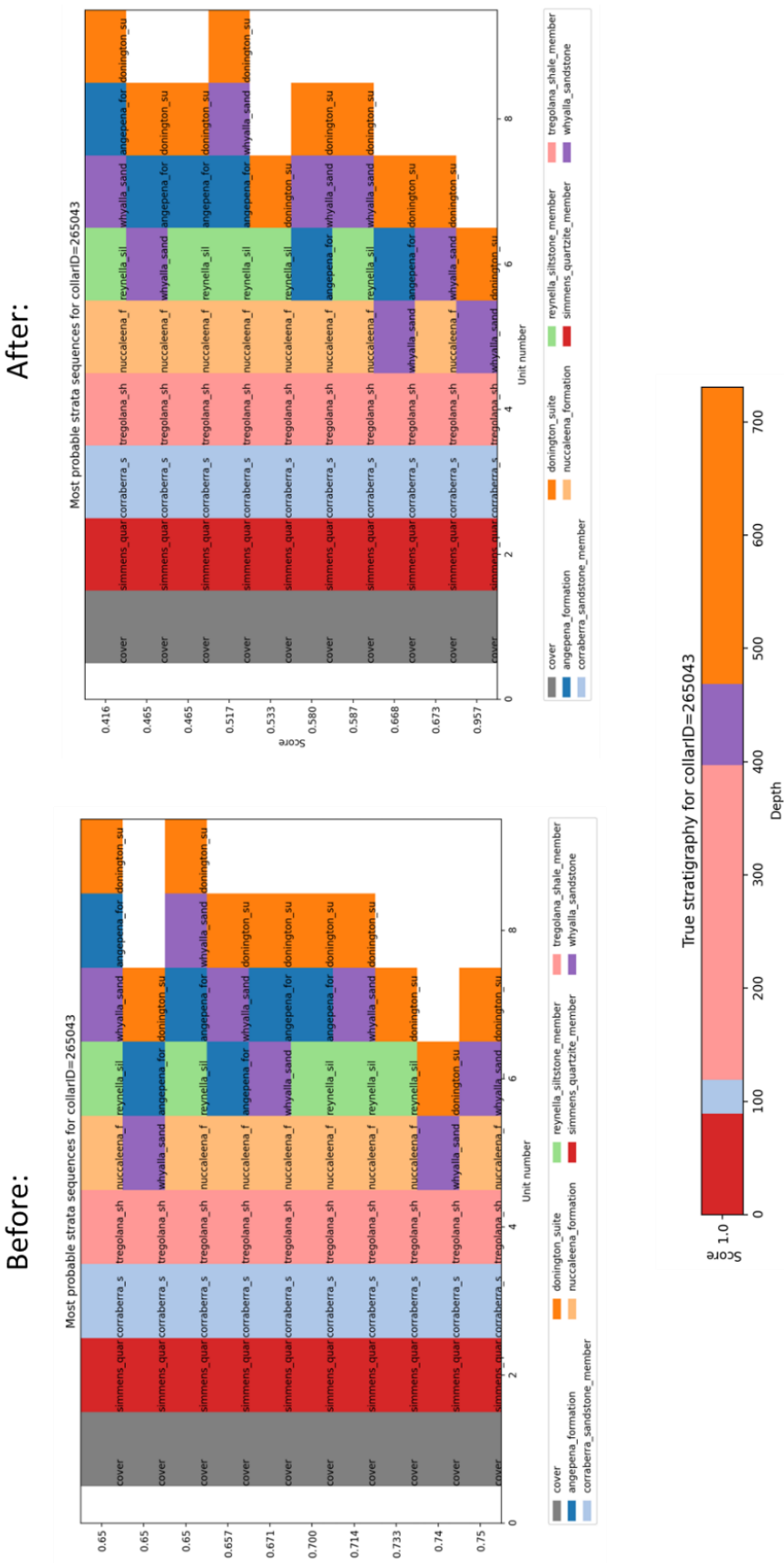


513

514 Figure 10: The 12 most probable stratigraphic orderings showing true depth of contact (above)
515 compared to the stratigraphy as logged for the same hole.

516

Figure 11: Comparison of ordering for one hole (left) vs ordering for that hole considering the outcomes of 45 other drillholes in the neighbourhood.



520

521 In the next stage of our analysis, we perform solution correlation across multiple drill holes to
522 establish a plausible stratigraphic order and reduce uncertainty. Figure 11 illustrates the comparison
523 of the most probable stratigraphies before and after correlation. Prior to correlation, the solution
524 that aligns with the “true” stratigraphy (the correct solution) is ranked second, with a score of
525 $S=0.74$, while the highest-ranked solution has a score of $S=0.75$. However, after applying the
526 correlation, the correct solution rises to the top rank with a score of $S=0.95$, whereas the previously
527 highest-ranked solution falls to second place with a score of $S=0.67$. This correlation analysis not only
528 helped identify the correct solution but also significantly reduced its relative uncertainty, increasing
529 the relative score between the top two solutions from 1% to 42%.

530 The computational efficiency of the litho2strat algorithm was evaluated through performance testing
531 on this dataset, with scalability analysis presented in Appendix B.

532

533 4. Discussion and Future Work

534

535 Whilst we were able to develop a workflow that successfully provided useful stratigraphic analyses
536 for our test area, we recognise that for other areas the methodology was not always as successful.
537 We have identified several aspects of the current stratigraphic descriptions that we think will
538 significantly expand the useability of the workflow we present above.

539 1) Lithological Uncertainty. The principal reason for this was that the lithological descriptions of
540 stratigraphies in many areas is quite vague. Successive stratigraphic units in a group might
541 have very similar lithological descriptions.

542 As an example, we look at the Hamersley Group, in Western Australia (Maldonado & Mercer,
543 2018). If we examine the GSWA explanatory notes for three successive formations (Mt McRae
544 Shale, Mt Sylvia Formation and the Wittenoom Formation) in the GSWA explanatory notes
545 their lithologies are described as:

- 546 • **Mt McRae Shale** - Mudstone, siltstone, chert, iron-formation, and dolomite. Thin
547 bands of shard-bearing volcanic ash in upper parts.
- 548 • **Mt Sylvia Formation** - Mudstone, siltstone, chert, iron-formation, and dolomite.
- 549 • **Wittenoom Formation** - Thinly bedded dolomite and dolomitic shale, with minor
550 black chert, shale, banded iron formation and sandstone.

551 We can see that there is a significant overlap in lithologies, with an ordering of lithologies but
552 without constraints on the percentage of each lithology in the three formations. This
553 additional information, even as an estimate, would provide useful constraints on the likelihood
554 that a specific lithology is associated with a given stratigraphic unit.

555

- 556 2) Min-Max thickness estimates. In some areas, there is useful information on the minimum,
557 maximum and average stratigraphic thickness of units.
- 558 3) Stratigraphic ordering of lithologies. Additional information on commonly occurring orderings
559 of lithologies within a given formation or member would also provide useful constraints.

West Angela Member

Derivation of name/Formal lithostratigraphy

The West Angela Member was the first subdivision of the Wittenoom Formation to be formally recognized (Blockley et al., 1993). It is named after West Angela Hill (Zone 50, MGA 673387E 7442407N) near the West Angelas iron ore mine, and the type section is defined as the interval between 420.4 m and 524.6 m in drill hole WRL 1 (Blockley et al., 1993) stored at the Geological Survey of Western Australia (GSAWA) [Carlisle Core Library](#).

Five shaly horizons separated by BIF, chert, or massive dolomite are recognized in the West Angela Member and are informally designated as AS1 to AS5 (Kepert, 2018). In particular the lower three shale horizons form a distinctive pattern in natural gamma-ray logs that can be used for regional correlation (Blockley et al., 1993).

<i>Minimum thickness (m)</i>	—
<i>Maximum thickness (m)</i>	80

Lithology

The West Angela Member is generally not well-exposed and consists predominantly of dolomite and shaly dolomite, with minor chert, BIF, volcanoclastic rocks, and impact ejecta layers. Near the base, there is a distinctive unit of interbedded chert, BIF, dolomitic shale, and shale with characteristic natural gamma-ray peaks that are designated AS1 to AS3 (Blockley et al., 1993). This entire interval is referred to as A1 by some mining companies (e.g. Kepert, 2018) and is overlain by a thick interval of shale and dolomitic shale (AS3). The middle of the member, between AS3 and AS 4, contains a unit of massive to laminated crystalline dolomite with local carbonaceous shale and siltstone partings (Blockley et al., 1993). The upper part of the West Angela Member (AS4 to AS5) consists mainly of dolomitic shale and shale with minor chert beds that is gradationally overlain by massive dolomite at the base of the Paraburadoo Member. Lateral correlations between drillholes WRL 1 and FVG 1 suggest that the member becomes shaler towards the east (Blockley et al., 1993).

563 Figure 12: Free-text descriptions of the West Angela Member in the GSWA Explanatory Notes.

564 All three of these types of information are often included in the free-text portions of stratigraphic
 565 databases, such as the example shown for the West Angela Member in the GSWA Explanatory
 566 Notes in Fig. 12. In this example the free text provides more specific information on the thickness,
 567 the ordering of lithologies and the relative proportions of lithologies. With the advent of more
 568 sophisticated Machine Learning methodologies, the extraction of this ancillary data in a
 569 standardised form from reports and the stratigraphic databases themselves will open up new
 570 possibilities for constraining stratigraphy. Similarly, the codes developed in dh2loop for
 571 harmonising lithological terminologies will expand greatly in coming years.

572 4) Inclusion of discontinuity information in the litho2strat workflow (most often logged faults)
 573 could help to define where breaks in stratigraphy are most likely to occur

574

575 5) Inclusion of secondary descriptive information (for example grain size) could help to refine our
 576 younging estimators in areas of uncertain facing.

577

578 6) There is no doubt that the advent of Large Language Models will have a profound effect on
 579 our ability to extract and categorize information from unstructured data sources, and
 580 algorithms based on these approaches will probably replace the data extraction and data
 581 harmonisation modules in future versions of this workflow.

585 5. Conclusions

586

587 We developed codes and methodologies for stratigraphy recovery from drillhole databases, utilizing
588 the branch and prune algorithm as a foundational framework. To ensure the generation of
589 geologically plausible solutions, we implemented various types of constraints that account for the
590 complexities of subsurface geology.

591 To further reduce uncertainty in the obtained solutions, we introduced a correlation algorithm that
592 leverages information from multiple drillholes simultaneously. This innovative approach allows for a
593 more robust analysis by integrating data across different locations, enhancing the reliability of the
594 stratigraphic interpretations.

595 Our proposed method was applied to a dataset comprising 52 drillholes from South Australia. The
596 results demonstrated that the algorithm successfully predicts the correct stratigraphic solution while
597 providing associated uncertainty metrics, effectively validating its performance against measured
598 stratigraphy data.

599 Additionally, we identified several key aspects of the current stratigraphic descriptions that could
600 significantly enhance the usability of the workflow we have presented. These enhancements aim to
601 improve the accessibility and applicability of our methodology, paving the way for more effective
602 geological assessments and decision-making processes in the field.

603

604

605

606

607

608

609

610

611

612

613

614

615

616

617

618

619

620 *Code and data availability.* The software and datasets used in this study are publicly available for
621 download at GitHub (<https://github.com/Loop3D/litho2strat>) and Zenodo
622 (<https://doi.org/10.5281/zenodo.15064469>, Ogarko et al., 2025).

623 *Author contribution.* VO and MJ are the primary contributors to this study. VO led the research,
624 developed the methodology and software, and prepared the manuscript. MJ provided guidance on
625 drillhole data analysis and contributed to manuscript writing.

626 *Competing interests.* The authors declare that they have no conflict of interest.

627 *Acknowledgements.* The work has been supported by the Mineral Exploration Cooperative Research
628 Centre whose activities are funded by the Australian Government's Cooperative Research Centre
629 Program. This is MinEx CRC Document 2025/27. We are grateful to reviewer Guillaume Caumon for
630 very helpful comments that greatly improved the paper.

```

631 Appendix A- Control file for litho2strat code
632
633 Example usage: python3 litho2strat.py -p ./parfiles/Parfile_SA.txt
634 Example parfile:
635
636     [FilePaths]
637     topology_filename = data/SA_test_data/newpairs_20_06_2023.gml
638     ignore_list_filename = data/SA_test_data/ignore_list.txt
639     alternative_rock_names_filename = data/SA_test_data/alternative_rock_names.txt
640     unit_colors_filename = data/SA_test_data/unit_colors.csv
641
642     drillsample_filename = data/SA_test_data/litho_tables/litho_${collarID}.csv
643     stratasample_filename = data/SA_test_data/strat_tables/strat_${collarID}.csv
644     dist_table_filename = data/SA_test_data/dh_asud_strat2.csv
645
646     [DataHeaders]
647     drillsample_header = DEPTH_FROM_M, DEPTH_TO_M, MAJOR_LITHOLOGY,
648     stratasample_header = DEPTH_FROM_M, DEPTH_TO_M, STRAT_UNIT_NAME,
649     strata_data_header = strat, summary, distance, description
650
651     [SolverParameters]
652     add_topology_constraints = True
653     max_num_strata_jumps = 0
654     max_num_returns_per_unit = 0
655     max_num_unit_contacts_inside_litho = 0
656     single_top_unit = True
657
658     [DataPreprocessing]
659     number_nearest_units = 10
660     min_drillhole_litho_score = 80
661     group_drillhole_lithos = False
662     cover_ratio_threshold = 0.65
663
664     [CollarIDs]
665     collarIDs = 205821,205822,264999,265000,265001

```

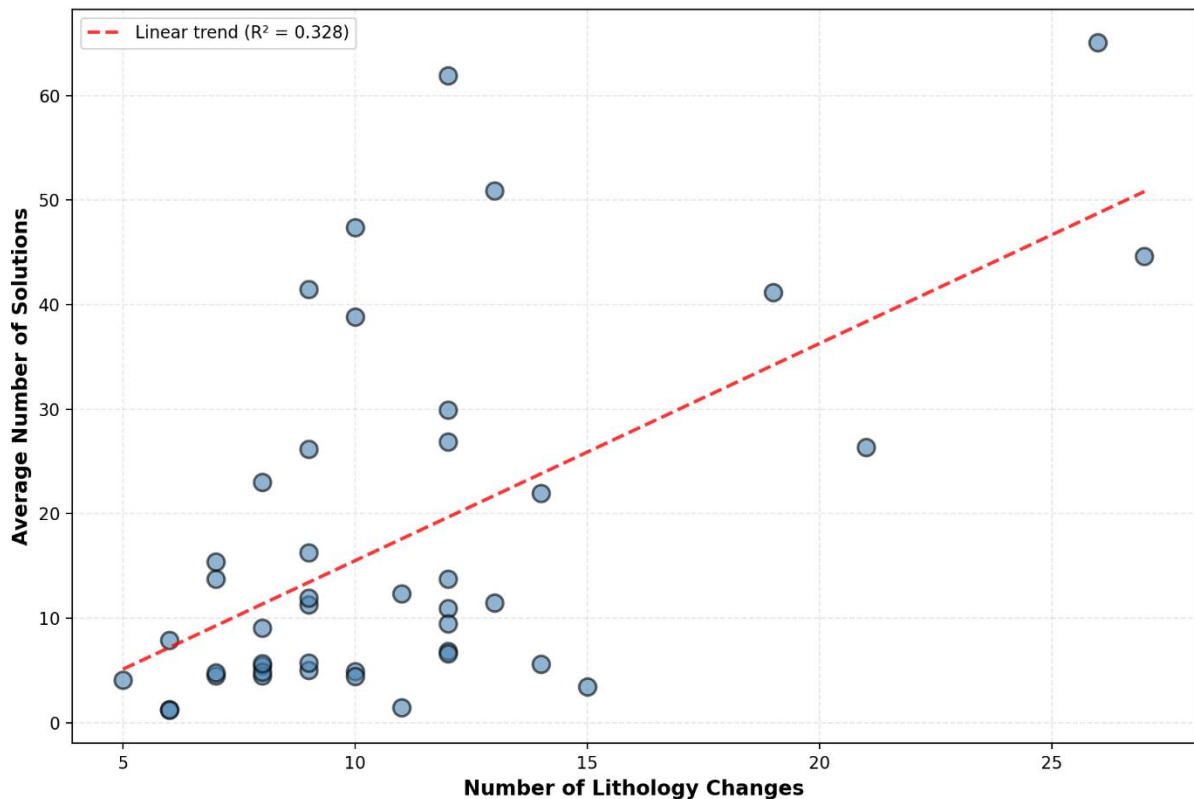
666 Appendix B: Performance and Scalability Analysis

667

668 To complement the theoretical complexity analysis presented in Section 2.4, we conducted empirical
669 tests to evaluate the performance and scalability of the litho2strat algorithm. We tested how the
670 average number of solutions maintained during recursive exploration (N) scales with the number of
671 lithology changes in drillhole logs, comparing two scenarios: (1) using the global topology graph Γ as
672 a constraint, and (2) without topology constraints.

673 Figure B.1 shows the relationship between the number of lithology changes and the average number
674 of solutions maintained during recursive exploration when the topology graph constraint is applied.
675 The results demonstrate near-linear scaling, confirming that the topology graph effectively prunes
676 the solution space while preserving geological validity.

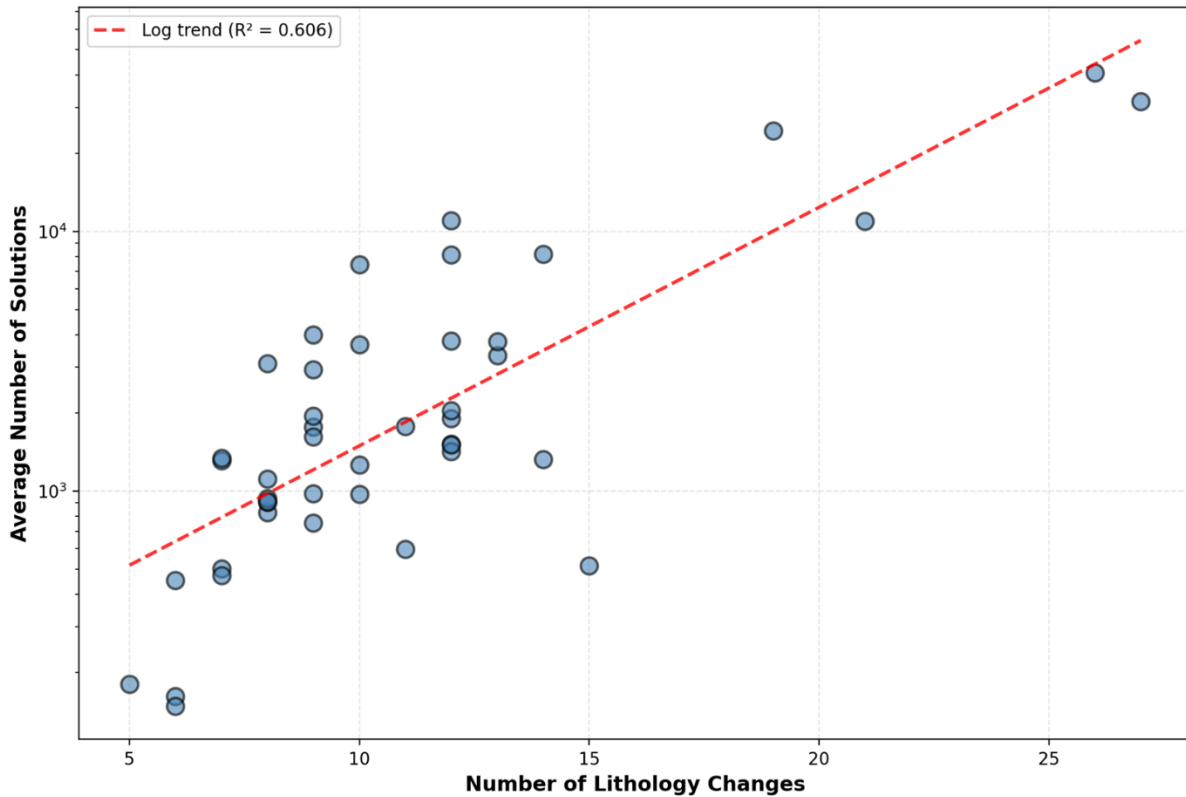
677



678

679 Figure B.1: Average number of solutions maintained during recursive exploration versus number of
680 lithology changes with topology graph constraint.

681 Figure B.2 presents the same relationship for the unconstrained case, where the algorithm considers
682 all theoretically possible stratigraphic interpretations. Here, the average number of solutions
683 maintained during recursive exploration exhibits near-exponential growth with increasing lithology
684 changes, illustrating the combinatorial explosion that occurs without geological constraints.



685

686 Figure B.2: Average number of solutions maintained during recursive exploration versus number of
687 lithology changes without topology constraints.

688 The computational performance measurements further highlight the practical importance of these
689 constraints. Using a single CPU core (Intel i7-1185G7 @ 3.00GHz) to process all 52 drillholes from
690 Section 3 and perform the correlation of solutions, the constrained approach required approximately
691 1 second total processing time, while the unconstrained case required approximately 50 seconds for
692 the same dataset. This 50-fold improvement in computational efficiency, combined with the near-
693 linear versus near-exponential scaling behavior of solutions maintained during recursive exploration,
694 demonstrates that incorporating geological knowledge through the topology graph is essential for
695 both computational tractability and practical applicability of the litho2strat algorithm to real-world
696 geological datasets.

697

698

699

700

701

702

703

704

705

706

707 Alvarado-Neves, F., Ailleres, L., Grose, L., Cruden, A. R., & Armit, R. (2024). Three-dimensional
708 geological modelling of igneous intrusions in LoopStructural v1.5.10. *Geoscientific Model
709 Development*, 17(5), 1975–1993. <https://doi.org/10.5194/gmd-17-1975-2024>

710 Calcagno, P., Chilès, J. P., Courrioux, G., & Guillen, A. (2008). Geological modelling from field data and
711 geological knowledge. *Physics of the Earth and Planetary Interiors*, 171(1–4), 147–157.
712 <https://doi.org/10.1016/j.pepi.2008.06.013>

713 Caumon, G., Collon-Drouaillet, P., Le Carlier de Veslud, C., Viseur, S., & Sausse, J. (2009). Surface-
714 Based 3D Modeling of Geological Structures. *Mathematical Geosciences*, 41(8), 927–945.
715 <https://doi.org/10.1007/s11004-009-9244-2>

716 D’Affonseca, F. M., Finkel, M., & Cirpka, O. A. (2020). Combining implicit geological modeling, field
717 surveys, and hydrogeological modeling to describe groundwater flow in a karst aquifer.
718 *Hydrogeology Journal*, 28(8), 2779–2802. <https://doi.org/10.1007/s10040-020-02220-z>

719 Fullagar, P.K., Zhou, B., and Biggs, M., 2004. Stratigraphically consistent autointerpretation of
720 borehole data. *Journal of Applied Geophysics*, 55(1-2), 91-104.
721 <https://doi.org/10.1016/j.jappgeo.2003.06.010>

722 Giraud, J., Pakyuz-Charrier, E., Jessell, M., Lindsay, M., Martin, R., & Ogarko, V. (2017). Uncertainty
723 reduction through geologically conditioned petrophysical constraints in joint inversion.
724 *GEOPHYSICS*, 82(6), ID19–ID34. <https://doi.org/10.1190/geo2016-0615.1>

725 Guo, J., Wang, Z., Li, C., Li, F., Jessell, M. W., Wu, L., & Wang, J. (2022). Multiple-Point Geostatistics-
726 Based Three-Dimensional Automatic Geological Modeling and Uncertainty Analysis for
727 Borehole Data. *Natural Resources Research*, 31(5), 2347–2367.
728 <https://doi.org/10.1007/s11053-022-10071-6>

729 Guo, J., Xu, X., Wang, L., Wang, X., Wu, L., Jessell, M., Ogarko, V., Liu, Z., & Zheng, Y. (2024). GeoPDNN
730 1.0: a semi-supervised deep learning neural network using pseudo-labels for three-dimensional
731 shallow strata modelling and uncertainty analysis in urban areas from borehole data.
732 *Geoscientific Model Development*, 17(3), 957–973. <https://doi.org/10.5194/gmd-17-957-2024>

733 Hagberg, A. A., Schult, D. A., & Swart, P. J. (2008). *Exploring Network Structure, Dynamics, and
734 Function using NetworkX*. 11–15. <https://doi.org/10.25080/TCWV9851>

735 Hartmann, J., & Moosdorf, N. (2012). The new global lithological map database GLiM: A
736 representation of rock properties at the Earth surface. *Geochemistry, Geophysics, Geosystems*,
737 13(12). <https://doi.org/10.1029/2012GC004370>

738 Hill, E.J., Pearce, M.A. & Stromberg, J.M. Improving Automated Geological Logging of Drill Holes by
739 Incorporating Multiscale Spatial Methods. *Math Geosci* 53, 21–53 (2021).
740 <https://doi.org/10.1007/s11004-020-09859-0>

741 Himsolt, M. (1997). *GML: a portable graph file format*.

742 Jessell, M. (2001). Three-dimensional geological modelling of potential-field data. *Computers &
743 Geosciences*, 27(4), 455–465. [https://doi.org/10.1016/S0098-3004\(00\)00142-4](https://doi.org/10.1016/S0098-3004(00)00142-4)

744 Jessell, M., Aillères, L., Kemp, E. de, Lindsay, M., Wellmann, F., Hillier, M., Laurent, G., Carmichael, T.,
745 & Martin, R. (2014). Next Generation Three-Dimensional Geologic Modeling and Inversion. In

746 *Building Exploration Capability for the 21st Century*. Society of Economic Geologists.
747 <https://doi.org/10.5382/SP.18.13>

748 Jessell, M., Ogarko, V., de Rose, Y., Lindsay, M., Joshi, R., Piechocka, A., Grose, L., de la Varga, M.,
749 Ailleres, L., & Pirot, G. (2021). Automated geological map deconstruction for 3D model
750 construction using <i>map2loop</i> 1.0 and
751 <i>map2model</i> 1.0. *Geoscientific Model Development*,
752 14(8), 5063–5092. <https://doi.org/10.5194/gmd-14-5063-2021>

753 Jessell, M. W., Ailleres, L., & de Kemp, E. A. (2010). Towards an integrated inversion of geoscientific
754 data: What price of geology? *Tectonophysics*, 490(3–4), 294–306.
755 <https://doi.org/10.1016/j.tecto.2010.05.020>

756 Joshi, R., Madaiah, K., Jessell, M., Lindsay, M., & Pirot, G. (2021).
757 <i>dh2loop</i> 1.0: an open-source Python library for
758 automated processing and classification of geological logs. *Geoscientific Model Development*,
759 14(11), 6711–6740. <https://doi.org/10.5194/gmd-14-6711-2021>

760 Land, A. H., & Doig, A. G. (1960). An Automatic Method of Solving Discrete Programming Problems.
761 *Econometrica*, 28(3), 497. <https://doi.org/10.2307/1910129>

762 Lindsay, M. D., Jessell, M. W., Ailleres, L., Perrouyt, S., de Kemp, E., & Betts, P. G. (2013). Geodiversity:
763 Exploration of 3D geological model space. *Tectonophysics*, 594, 27–37.
764 <https://doi.org/10.1016/j.tecto.2013.03.013>

765 Maldonado, A., & Mercer, K. (2018). *Comparison of the Laboratory and Barton-Bandis Derived Shear
766 Strength of Bedding Partings in Fresh Shales of the Pilbara, Western Australia. All Days*, ISRM-
767 ARMS10-2018-204.

768 Mallet, J.-L. L. (2002). *Geomodeling*. Oxford University Press, Inc.

769 Martin, R., Ogarko, V., Giraud, J., Plazolles, B., Angrand, P., Rousse, S., & Macouin, M. (2024). Gravity
770 data inversion of the Pyrenees range using Taguchi sensitivity analysis and ADMM bound
771 constraints based on seismic data. *Geophysical Journal International*, 240(1), 829–858.
772 <https://doi.org/10.1093/gji/ggae410>

773 Ogarko, V., Giraud, J., Martin, R., & Jessell, M. (2021). Disjoint interval bound constraints using the
774 alternating direction method of multipliers for geologically constrained inversion: Application to
775 gravity data. *GEOPHYSICS*, 86(2), G1–G11. <https://doi.org/10.1190/geo2019-0633.1>

776 Ogarko, V., & Jessell, M. (2025). litho2strat 1.0 source code,
777 <https://doi.org/10.5281/zenodo.15064469>

778 Pakyuz-Charrier, E., Giraud, J., Ogarko, V., Lindsay, M., & Jessell, M. (2018). Drillhole uncertainty
779 propagation for three-dimensional geological modeling using Monte Carlo. *Tectonophysics*,
780 747–748, 16–39. <https://doi.org/10.1016/j.tecto.2018.09.005>

781 Schetselaar, E. M., & Lemieux, D. (2012). A drill hole query algorithm for extracting lithostratigraphic
782 contacts in support of 3D geologic modelling in crystalline basement. *Computers & Geosciences*,
783 44, 146–155. <https://doi.org/10.1016/j.cageo.2011.10.015>

784 Silversides, K., Melkumyan, A., Wyman, D.A., and Hatherly, P., 2015. Automated recognition of
785 stratigraphic marker shales from geophysical logs in iron ore deposits. *Computers &
786 Geosciences*, 77, 118-125. <https://doi.org/10.1016/j.cageo.2015.02.002>

787 Tarantola, A. (2005). *Inverse Problem Theory and Methods for Model Parameter Estimation*. Society
788 for Industrial and Applied Mathematics. <https://doi.org/10.1137/1.9780898717921>

789 Vollgger, S. A., Cruden, A. R., Ailleres, L., & Cowan, E. J. (2015). Regional dome evolution and its
790 control on ore-grade distribution: Insights from 3D implicit modelling of the Navachab gold
791 deposit, Namibia. *Ore Geology Reviews*, 69, 268–284.
792 <https://doi.org/10.1016/j.oregeorev.2015.02.020>

793 Wedge, D., Hartley, O., McMickan, A., Green, T., and Holden, E., 2019. Machine learning assisted
794 geological interpretation of drillhole data: Examples from the Pilbara Region, Western Australia.
795 *Ore Geology Reviews*, 114, 103118. <https://doi.org/10.1016/j.oregeorev.2019.103118>

796 Wellmann, F., & Caumon, G. (2018). *3-D Structural geological models: Concepts, methods, and*
797 *uncertainties* (pp. 1–121). <https://doi.org/10.1016/bs.agph.2018.09.001>

798 Wu, X., and Nyland, E., (1987). Automated stratigraphic interpretation of well-log data. *Geophysics*,
799 52(12), 1665-1676. <https://doi.org/10.1190/1.1442283>

800